Journal of Fluorescence, Vol. 15, No. 5, September 2005 (© 2005)
DOI: 10.1007/s10895-005-2989-1

On the Quantitative Treatment of Donor–Donor Energy Migration in Regularly Aggregated Proteins

Denys Marushchak[1] and Lennart B.-Å. Johansson[1,2]

Received June 1, 2005; accepted July 26, 2005

An algorithm is presented that quantitatively accounts for donor–donor energy migration (DDEM) among fluorophore-labeled proteins forming regular aggregates. The DDEM algorithm is based on Monte Carlo and Brownian dynamics simulations and applies to calculation of fluorescence depolarisation data, such as the fluorescence anisotropy. Thereby local orientations, as well as reorienting motions of the fluorescent group are considered in the absence and presence of DDEM and among, in principle, infinitely many proteins as they form regular aggregates. Here we apply the algorithm for calculating and illustrating the DDEM and the time-resolved fluorescence anisotropy under static as well as dynamic conditions within helical, linear and circular aggregate structures. A principal approach of the DDEM algorithm for analysing protein aggregates is also outlined.

KEY WORDS: Protein aggregates; protein polymers; fluorescence anisotropy; donor–donor energy migration; homo transfer; amyloid diseases; Monte Carlo simulation; Brownian dynamics.

INTRODUCTION

Proteins may form oligomeres but also very large aggregates, which constitute a regular structure. For instance, transthyretin forms tetramers and mutants of transthyretin can form large aggregates, which are associated with the human amyloid disease, *familial amyloidic polyneuropathy* [1,2]. The formation of protein complexes is also connected with conformational diseases, such as the Alzheimer's and the Creutzfeldt-Jakob's diseases [3]. The actin-aggregation in muscle fibrils exemplifies another interesting system for which a structural model has been proposed [4,5] but which is not generally accepted. Cytolytic toxins associated with diseases in humans and animals [6,7] constitute other aggregating proteins which are thought to create pores in membranes [8]. Tubulin is yet another well-known protein that forms the building unit of microtubules (see e.g., [9]).

The molecular understanding of bioprocesses is intimately related to physico-chemical methods for obtaining structural and dynamic information about proteins and nucleic acids, etc. The traditional structural methods are based on X-ray diffraction and multidimensional NMR-spectroscopy. Electronic energy transfer between donor and acceptor groups [10,11] has also been used for years, as well as more recently energy transfer between identical fluorophores, so-called donor–donor energy migration (DDEM) [12]. All methods, however, show advantages and disadvantages. While X-ray-diffraction relies on the preparation of crystals of high quality, NMR may, for larger molecules, suffer in spectral resolution. On the other hand, detailed distance information can be obtained (Å-resolution) provided these problems are overcome. The distances obtained from studies of electronic energy transfer and DDEM experiments are much longer typically between 10 and 100 Å, and the methodological problems concern the specific labelling [12] and the quantitative molecular interpretation of data. The latter question, however, could be overcome by using a recent development of an extended Förster theory [13,14].

[1] Department of Chemistry; Biophysical Chemistry, University of Umeå, S-901 87 Umeå, Sweden.
[2] To whom correspondence should be addressed. E-mail: lennart.johansson @chem.umu.se

To characterise monomer/dimer transitions in solution, researchers have utilised the influence of DDEM on the fluorescence depolarisation [15–18]. Using the additivity of the fluorescence anisotropy, calculation of the fraction of each state becomes possible, provided one knows what kind of aggregates are formed. In many cases, however, the fluorescence depolarisation data contain additional structural information. Several scientists have also used energy transfer/migration for examining peptides and proteins in lipid bilayers and have been able to show nonuniform distributions [19–21].

This paper aims at showing how Monte Carlo (MC) simulations can be used to quantitatively describe the DDEM between fluorescent groups, which are specifically linked to stochastically distributed protein monomers in a regular aggregate. The presented algorithm accounts for local orientational restriction and motions of the fluorophore in the protein, as well as the geometrical parameters of different regular structures.

COMPUTER METHODS AND FACILITIES

Simulations of energy migration between fluorescent donors in proteins aggregate structures were performed to obtain the time-dependent fluorescence anisotropy *r(t)*. The so called "κ^2 problem" [14,22,23] is then an important question to account for accurately. The square of the angular part of the dipole-dipole coupling, $\langle\kappa^2\rangle$, is a function of the mutual orientation of the interacting dipole moments, as is obvious from Eq. (4) (*vide infra*). In cases when the rate of energy migration is much slower or faster than the fluorophore reorientation, the static or dynamic isotropic averages of $\langle\kappa^2\rangle$ are often used. In the present study no such approximations are assumed. Instead, the dynamic processes are allowed to occur on the same timescale. It is then necessary to use simulation methods that account for the reorienting motions of the fluorescent group, which moreover are restricted due to the binding to proteins. These conditions are achieved by Brownian Dynamics (BD) simulations, as described elsewhere [14]. In the simulations, a unit vector representing the molecular electronic transition dipole moment ($\vec{\mu}$) undergoes diffusion on a restricted part of a spherical surface, defined by a first rank Maier-Saupe potential.

The initial coordinates of the unit vector are generated by using the rejection method [24]. The numerical scheme uses a 3D-diffusion process, restricted to the two-dimensional surface of the sphere. Cartesian coordinates are used and the potential is transformed into coordinates that introduce a deterministic force in the BD-simulation. The main steps of the simulation algorithm are as follows:

1. Perform the labeling by choosing which of the adjacent protein monomers has a fluorophore attached, and then sample the initial coordinates of the dipole vectors $\vec{\mu}_i$.
2. For each dipole within a cut-off distance, meaning a certain number of protein neighbors (*N*, where *N* is usually nine proteins on each side), one performs a BD simulation of trajectory. Here the potential amplitude was $\gamma_1 = 14$ (*vide infra* Eq. (1)), which corresponds to a local order parameter of 0.80 and a rotational correlation time of 0.86 (in units of reduced time).
3. To determine $r(t)$ a MC simulation of energy migration is performed. This is further described in the section: Theoretical Prerequisites. The timescale was divided into 1024 channels with a channel width of $\Delta t = 0.00862$, that gives maximum simulation time, $T_\infty = 8.83$ (in units of reduced time).
4. The steps 1–3 are repeated several times (usually 100,000) in order to calculate the average $\langle r(t)\rangle$.

Because the resulting anisotropy is an average over a large ensemble of independent simulations, it is possible to perform parallel computer calculations. For this the MPI library was used. All the calculations were made on a cluster of 6 Linux computers, each with an AMD Sempron processor, under LAM. This cluster needs a few minutes to calculate one anisotropy decay, corresponding to about 1000 simulations. However the computational time depends on the fraction of labelling, as well as the strength of coupling.

THEORETICAL PRE-REQUISITES

Regular Protein Structures

In the modeling of regular protein aggregates we have concentrated on the helical structure, which has been proposed, for instance, for *F*-actin [4] and polymers of α1-antitrypsin [25,26]. This prototype structure is also interesting because it covers the special cases of linear and ring-shaped structures. The characteristic parameters of a helix (cf. Fig. 1) are composed of translational distance (T_z), the rotation (θ) of each neighbour protein, and the radial distance between the helical axis and the position of the fluorescent donor (T_{xy}). For the proposed structure of *F*-actin, the position of a the next monomer is obtained from the coordinates of the preceding one by an axial translation and a rotation of $T_z = 27.5$ Å and $\theta = 166^\circ$, respectively [5]. The distance between the helical axis and

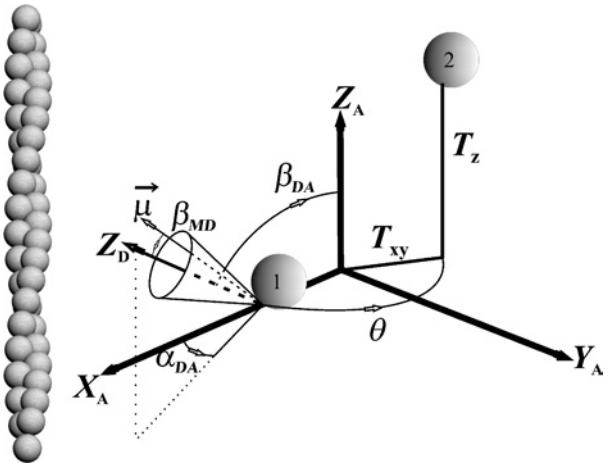

Fig. 1. Schematic showing the coordinate systems used to describe the protein position in regular structures forming helical, linear and ring-shaped aggregates. The Z_A axis coincides with the C_∞-axis of the aggregate and T_{xy} denotes the distance from this axis to the position of a fluorescent group. The translational and rotational transformations between nearest protein neighbours are θ and T_z, respectively. The fluorophore undergoes local reorienting motions about an effective symmetry axis Z_D that is transformed to the aggregate fixed frame by $\Omega_{DA} = (\alpha_{DA},\beta_{DA})$. The electric transition dipole $\vec{\mu}$ is transformed to the D-frame by the angles $\Omega_{DA} = (\alpha_{DA}, \beta_{DA})$.

the Cys-374 is of particular interest since this position can be labelled by a fluorescence group. The distance from the C_∞ axis to the centre of mass of the fluorescent group would then correspond to the T_{xy} in Fig. 1. Previously Moens *et al*. have reported $T_{xy} = 13.7$ Å [5].

In present work, one donor (D) group is covalently bonded to a protein molecule at a well-defined position in the structure. The local orientation of the D is assumed to be effectively uniaxial with respect to the Z_D (cf. Fig. 1) and the donor may also undergo interaction under conditions of reorienting motions ranging from static to dynamic. The latter means that energy migration between the D-groups is treated for negligible local motions as well as for motions that occur on the time scale of interaction, respectively. A Maier-Saupe potential given by

$$U(\beta_{MD}) = \gamma_1 P_1(\cos\ \beta_{MD}) \tag{1}$$

is used to describe restricted orientation and motion about the Z_D axis. Here $P_1(\cos\ \beta_{MD})$ is the first Legendre polynomial. Brownian dynamic (BD) simulations are applied to account for the local reorienting motions.

Because the protein aggregates are rather large, their tumbling motions are negligible on the timescale of most fluorescent molecules.

Energy Migration in Many-Donor Systems

Due to the extraordinary complexity in accounting for interactions among many donors, an analytical theoretical description does not exist for these systems. Additional difficulties are caused by the anisotropic orientation of the fluorophores and their internal motions. Here these questions are circumvented by using MC simulations. The MC simulation of energy migration involves all donor molecules within some cut-off distance, which is usually $\pm$ 9 protein molecules counted from the protein (number 0) that carries an excited donor. The total migration rate is calculated from

$$\Omega(t) = \sum_{j=-n}^{n} \omega_{0j}(t) \tag{2}$$

In Eq. (2) $\omega_{0j}(t)$ stands for the rate of energy migration from the 0:th to the *j*:th donor. This rate is given by the well-known Förster equation:

$$\omega_{0j}(t) = \frac{3\kappa_{0j}^2(t)}{2\tau}\left(\frac{R_0}{R_{0j}}\right)^6 \tag{3}$$

in which τ, R_0, R_{0j}, and κ_{0j}^2 denote the donor fluorescence lifetime, the Förster radius, the distance between the 0th to the *j*th donor, and the square of the angular part of the dipole–dipole coupling, respectively. The explicit expression for the latter reads:

$$\kappa_{0j}^2(t) = (\hat{\mu}_0(t)\cdot\hat{\mu}_j(t) - 3\{\hat{\mu}_0(t)\cdot\hat{R}_{0j}\}\{\hat{\mu}_j(t)\cdot\hat{R}_{0j}\})^2 \tag{4}$$

In Eq. (4) $\hat{\mu}_k$ and $\hat{R}_{0j}$ are unit vectors of the electronic transition dipoles and a distance vector between the centra of mass of the 0th and *j*th donor, respectively.

The coordinates of $\hat{\mu}_j$ with respect to the aggregate fixed frame are given by $\hat{\mu}_j(t) = \vec{A}_{\mu_j}(t) - \vec{O}(T_{xy}, T_z, \theta, j)$, where $\vec{A}_{\mu_j}(t)$ and $\vec{O}(T_{xy}, T_z, \theta, j)$ denote the vector pointing from the origin of X_A, Y_A, Z_A to the point described by $\hat{\mu}_j$ and the position of the centre of mass of the *j*th donor, respectively (cf. Fig. 1).

The first question to solve in the MC simulation is *when* an energy migration event takes place, denoted τ_{EM}. We chose a time interval Δt that is smaller than the characteristic time for the variation of $\Omega(t)$ caused by reorienting motions. It means that $\Omega(t)$ is approximated to be a constant within the time interval Δt. Then we generate a random number from a uniform distribution$\eta \in (0, 1]$, and calculate the time τ_{EM} according to

$$\tau_{EM} = -\frac{1}{\Omega(t)}\ln\ \eta \tag{5}$$

The obtained value will only be accepted provided $\eta < \Delta t$, which would ensure that $\Omega(t)$ can be considered constant. If $\eta > \Delta t$ one may step forward a time unit Δt and calculate $\Omega(t + \Delta t)$. Using this Ω-value a new random number is generated. This procedure is repeated until one finds a value of $\eta < \Delta t$.

The second decision concerns *where* the energy migrates, i.e. to which D group among the labelled proteins. From the above calculations one knows the time (T) of the energy migration event. By using BD simulations we can therefore account for the reorienting motions of all donors within the cut-off distance $\vec{A}_{\mu_j}(T)$. This enables the calculation of $\kappa^2_{0j}(T), \omega_{0j}(T)$ as well as $\Omega(T)$. The simulation of the orientational trajectories is for all particles performed in time window $T \in [0, T_\infty]$ within the cut-off distance, and it is only repeated when moving along the aggregate. To select the coming excited donor we normalize energy migration rates and sort it in decreasing order according to

$$|\omega_{0j}(T)| = \frac{\omega_{0j}(T)}{\Omega(T)} \tag{6}$$

We then generate a random number from a uniform distribution $\eta \in (0, 1]$, and select the ith donor for which

$$\eta \in \left(\sum_{j=1}^{j=i-1} \omega_{0j}(T), \sum_{j=1}^{j=i} \omega_{0j}(T) \right] \tag{7}$$

The calculations above (Eqs. (2)–(5)) account for local anisotropic motions of the donors groups, i.e. energy migration under dynamic conditions. For energy migration in the static limit the scheme also holds, but the time-dependence of ω_{0j} and Ω is, of course no longer relevant.

The time-dependent fluorescence anisotropy ($r(t)$) is calculated for times $[T - \tau, T)$ following the above scheme until one reaches the time $T \geq T_\infty$. Moreover the procedure is repeated many times before the forming the following final ensemble average ($= \langle \cdots \rangle$):

$$r(t) = r_0 \sum_j \langle p_j(t) P_2(\hat{\mu}_0(0)\hat{\mu}_j(t)) \rangle \tag{8}$$

In Eq. (8) the subfix j runs over all proteins, e.g. from -200 to $+200$ depending on the aggregate examined with the probability $p_j(t) = 1$ if the jth donor is excited and 0 otherwise. $P_2(\hat{\mu}_0(0)\hat{\mu}_j(t))$ is the second Legendre polynomial.

RESULTS AND DISCUSSION

This section is outlined as follows. After presenting different test cases of the algorithm, we describe and exemplify its versatility, and show how it can be applied to the analyses of true experimental data. In the final section we discuss the principle use of the DDEM algorithm for extracting structural information by comparing experimental depolarisation data with the simulated.

Tests of the DDEM Algorithm

Different cases were selected for testing the DDEM algorithm. To start with, we have considered DDEM within oligomers, i.e. dimers, trimers, tetramers and N-mers, for which all proteins are identically labelled with respect to position and orientation. The time-dependent fluorescence anisotropy will then reach a plateau value $\{r(t_\infty)\}$ which in the static limit is

$$r(t_\infty) = r_0 \frac{\sum_{j=0}^{N-1} P_2(\hat{\mu}_0 \cdot \hat{\mu}_j)}{N} \tag{9}$$

The limiting anisotropy values, calculated and simulated, are summarised in Table I. Different spatial configurations of dimers, trimers, tetramers and pentamers are studied. There is a good agreement with deviations typically less than the errors of experimental determinations.

For a dimer the time-dependent fluorescence anisotropy in the static limit is given by the following analytical expression [28]:

$$r(t) = ((r_0 - r_\infty)\exp(-2\omega t) + r_\infty) f + r_0(1 - f) \tag{10}$$

where f is the labelling probability. The results obtained when comparing DDEM simulations and Eq. (10) for different labelling probabilities show an excellent agreement. The small deviations depend on the statistical noise which

Table I. The Calculated $\{r_{\text{calc}}(t_\infty)$ Using Eq. (9)$\}$ and DDEM-Simulated $\{r(t_\infty)\}$ Limiting Fluorescence Anisotropy Values for DDEM Within Different D-labeled Oligomers (dimer-Pentamers) in the Static Case

Spatial configuration	$r(t_\infty)$	$r_{\text{calc}}(t_\infty)$
XO	0.3637	0.3637
OXO	0.3582	0.3582
XOO	0.3279	0.3281
XOOO	0.2784	0.2784
OXOO	0.3308	0.3329
XOOOO	0.2208	0.2215

Note. For describing various spatial configurations, X denotes that the donor is initially excited, and label O means a labeled neighbour. In the calculations of the limiting anisotropy the following data were used for helical aggregates:$\omega = 0.6093$, $(\hat{\mu}_0 \cdot \hat{\mu}_1) = -0.9709$, $(\hat{\mu}_0 \cdot \hat{\mu}_2) = 0.8855$, $(\hat{\mu}_0 \cdot \hat{\mu}_3) = -0.7486$, $(\hat{\mu}_0 \cdot \hat{\mu}_4) = 0.5682$.

is considerably reduced by averaging over 100,000 instead of 10,000 simulations (See Fig. 2.)

For high rates of DDEM over large distances in a helical structure, the orientational distribution of excited donors becomes cylindrically symmetric about the C_∞-axis with time. Provided that the local rotational correlation times are short, the time-dependent fluorescence anisotropy reaches a residual plateau value:

$$r(t_\infty) = r_0[3\cos^2\ \beta_{\mathrm{DA}}\cos\ 2\alpha_{\mathrm{DA}} - 3\sin^2\ \beta_{\mathrm{DA}} + 1] \times \frac{\langle D_{00}^{(2)}(\beta_{\mathrm{MD}})\rangle^2}{4} \tag{11}$$

here $\langle D_{00}^{(2)}(\beta_{\mathrm{MD}})\rangle$ describes the local order of the donor transition dipole with the respect to the Z_{D}-axis of the local frame (cf. Fig. 1). The other angles are defined in Fig. 1. The $r(t_\infty)$-values obtained by using the DDEM algorithm and Eq. (11) for various configurations (see Table II) show convincing agreement.

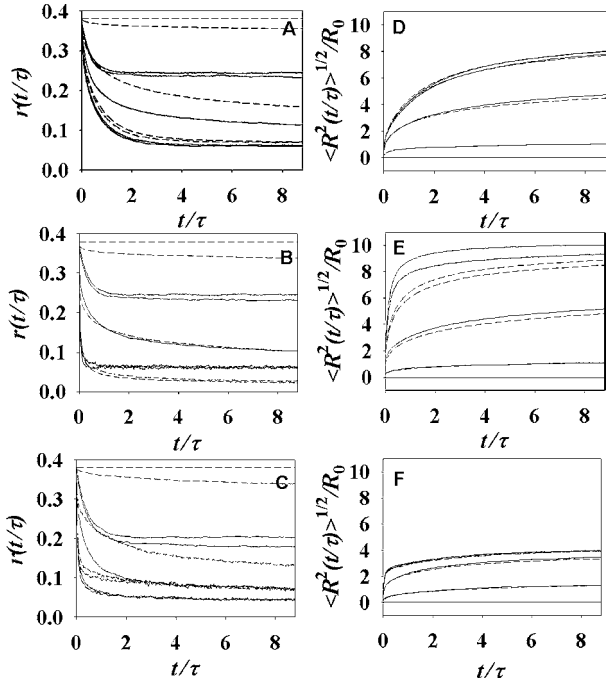

Fig. 2. The time-dependent anisotropy decay $\{r(t)\}$ obtained with the DDEM algorithm for the case of two neighbouring proteins that are labelled with the probabilities (= *f*) 0, 10, 50, 90, and 100% (solid line). For a comparison, the analytical solutions calculated (cf. Eq. (10)) for the corresponding *f*-values are also plotted (dotted line). The ensemble average includes more than 10,000 simulations, except for $f = 100\%$ where more than 100,000 simulations were performed. The insert compares the $r(t)$-values obtained with the analytical theory (·····) and the DDEM algorithm averaged over 10,000 (——) and 100,000 (—) simulations. The $\Delta r(t)$ ranges between 0.3634 and 0.3640. All data refer to DDEM in the static limit.

Table II. The Calculated $\{r_{\mathrm{calc}}(t_\infty)$ Using Eq. (11)$\}$ and DDEM-Simulated $\{r(t_\infty)\}$ Limiting Fluorescence Anisotropy Values are Displayed for Different Configurations (α_{MD}, β_{MD})

α_{MD} (°)	β_{MD} (°)	$r(t_\infty)$	$r_{\mathrm{calc}}(t_\infty)$
0	90	0.0613	0.0609
0	120	0.0038	0.0038
30	120	0.0114	0.0117
30	135	0.0012	0.0009
45	135	0.0037	0.0038
45	150	0.0018	0.0009
10	170	0.2004	0.2073
25	175	0.1254	0.1265
90	180	0.0608	0.0616

Note. The donor groups undergo Brownian motion in a Maier-Saupe potential with the parameter $\gamma_1 = 14$. In the absence of DDEM $r(t_\infty) = 0.2450 \pm 0.0025$.

The Aggregate Symmetry and *r(t)*

Three principal aggregate symmetries are considered namely; the helical, linear, and circular one. To illustrate the influence of aggregate symmetry on the time-resolved fluorescence depolarisation, data were generated for the same configuration ($\alpha_{\mathrm{DA}}, \beta_{\mathrm{DA}}$) and local order ($\langle D_{00}^{(2)}(\beta_{\mathrm{MD}})\rangle$) of the donor group, as well as for different labelling efficiencies. The influence of dynamics was also examined. The data suggest (see Fig. 3) that the energy migration in the static limit is faster in linear and circular aggregates as compared to the helical geometry. More evident is the large difference between the $r(t)$-decays in the static limit, at low degrees of labeling (*f*), and in the presence of reorienting motion of the donor groups. With increasing *f*-values, however, this difference decreases so that the $r(t)$-decays become very similar for *f*-values approaching 100%. The simulations with the DDEM algorithm also provide information about how far the initially excited energy migrates within the aggregate. In units of average number of Förster radii we find that the migration in the linear aggregate is much faster and takes place over a larger distance as compared to the helical aggregate. This is compatible with the difference in dimensionality and a similar behaviour has also been observed [28]. Because the energy displacement in a ring is directly related to its radius a comparison is less straightforward between the circular geometry on one hand, and the helical and linear geometries, on the other.

The DDEM Algorithm and the Analyses of Depolarisation Data

The number of parameters needed to describe the aggregate structure (T_{xy}, T_z, θ), the static ($\alpha_{\mathrm{DA}}, \beta_{\mathrm{DA}}$,

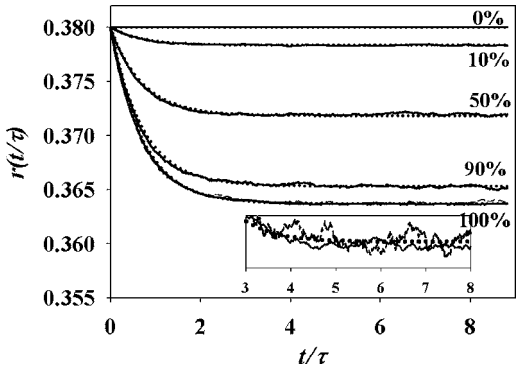

Fig. 3. The time-dependent anisotropy decay $\{r(t)\}$ and the normalised mean square displacement of the excitation $\{\langle R^2(t)\rangle^{1/2}/R_0\}$. The unit on the x-axis is reduced time, i.e. t/τ where τ is the fluorescence lifetime. The data refers to the following aggregate geometries: helical **(A, D)**, linear **(B, E)** and circular **(C, F)**. The dashed lines correspond to DDEM in the static limit (for local uniaxial anisotropic D-distribution), while the remaining $r(t)$-decays (solid lines) account for Brownian motions within the corresponding uniaxial Maier-Saupe potentials. The rotational correlation time is 0.86 in units of reduced time. In graphs **A, B** and **C** the residual anisotropy $\{r(t_\infty)\}$ decreases, while the mean square displacement **(D, E, F)** increases with increasing fraction of labelling. The labelling fractions (f) start by a very low value ($f \approx 10^{-4}$) and are increased to 5, 50, 95, and 100%. The local order parameter $\langle D_{00}^{(2)}(\beta_{\mathrm{MD}})\rangle = 0.80$.

$\langle D_{00}^{(2)}(\beta_{\mathrm{MD}})\rangle$) and dynamic (rotational correlation time) properties of the donor group are typically seven. The configuration parameters α_{DA}, β_{DA} have a large influence on the anisotropy, which for the static case, as well as in the presence of reorientation is illustrated in Fig. 4. In order to entirely determine the parameter space, one needs to increase the information content of the data analysed by conducting a number of linearly independent experiments. This can be possible by varying the fraction (f) of donor-labelled proteins in the aggregate, since the $r(t)$-decays evidently depend strongly on f, as illustrated in Fig. 3. For sufficiently low f-values energy migration between the D-groups becomes negligible, which implies that the time-resolved fluorescence anisotropy reveals information about order and dynamics of non-interacting donors. This information is used to determine properties of a particular local orienting potential [14]. As a consequence, knowledge about the local order parameter and the rotational correlation time reduces the number of unknown parameters to five. It is reasonable to assume that the potential is also relevant in the presence of DDEM. In the remaining analyses the unknown parameters could then be determined by analysing all of the linearly independent experiments in a global manner. The overall flow scheme for using the DDEM algorithm in the analyses of depolarisation data is presented in Fig. 5.

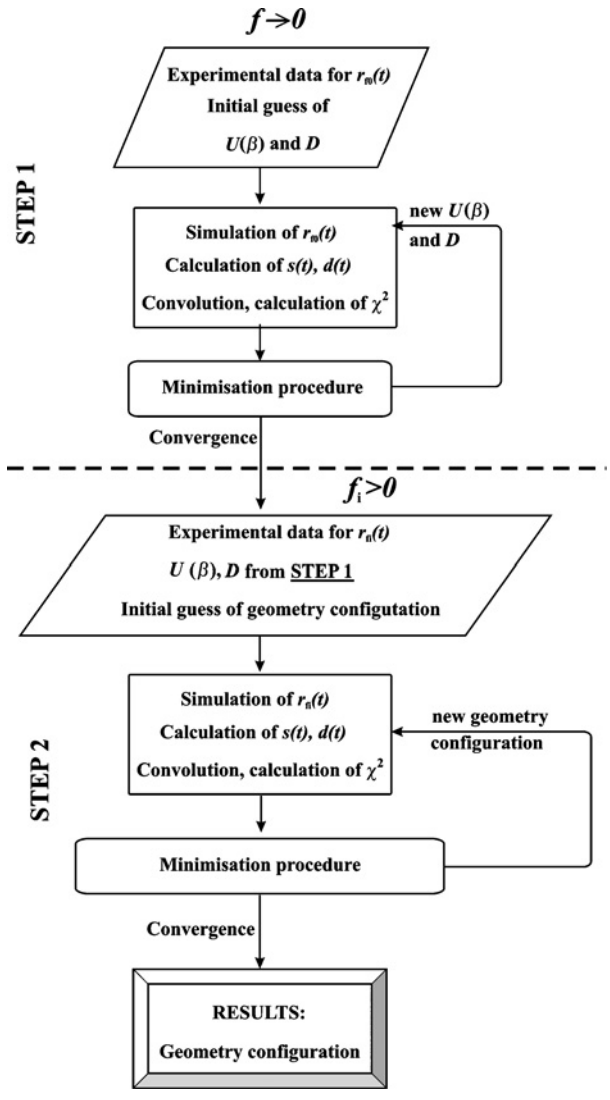

Fig. 4. The time-resolved fluorescence anisotropy $\{r(t)\}$ of donors localised in helical forming protein aggregates is displayed as a function of the configuration angle β_{DA}. The upper and lower anisotropy surfaces are obtained under static conditions and in the presence of local reorienting motions, respectively. The labeling fraction is 43%, the rotational correlation time is 0.86 in units of reduced time, the local order parameter $\langle D_{00}^{(2)}(\beta_{\mathrm{MD}})\rangle = 0.80$, and $\alpha_{\mathrm{DA}} = 0^\circ$.

CONCLUDING REMARKS

A DDEM algorithm has been developed, presented, tested and illustrated. It accounts for DDEM within regular aggregate structures, which may in practice be regarded as infinite. Furthermore it accounts for the local anisotropic order and reorienting motions of the D-groups in a protein. In this study we used information in the choice of parameters that are relevant for the local order and dynamics, as well as the fluorescence lifetime. These data

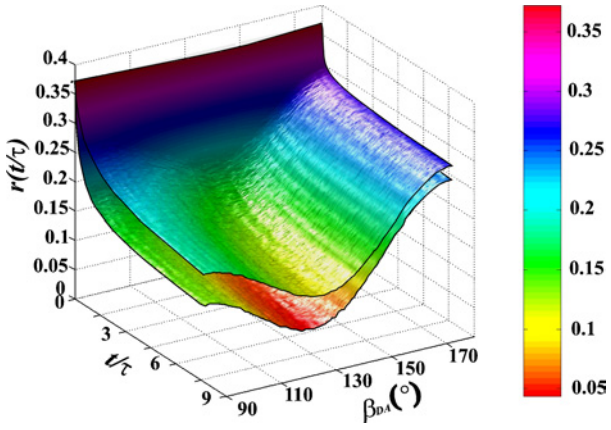

Fig. 5. A flow scheme describing the simulation-deconvolution DDEM algorithm. First one analyses experimental data that are obtained from measurements on aggregates with a low fraction of labelling, i.e. $f \to 0$. Using guessed parameters on the orienting potential $\{U(\beta_{\mathrm{MD}})\}$ and the diffusion constant $\{D\}$ that mimic experimental data are simulated and compared with the true experimental data, in a repetitive manner until convergence and the best statistical fit is achieved. This procedure involves the simulation of $r_{f0}(t)$, the calculation of the sum and difference curves $\{s(t), d(t)\}$, the convolution with an experimental response function, and the statistical analyses (χ^2, etc.) of the data. This leads to determining $U(\beta_{\mathrm{MD}})$ and D, which are pre-requisites for the next step in the analysis. The experimental data depend on DDEM and are obtained for different fractions of labelling, and then pass into another fitting routine. In this procedure the parameters describing the geometry and configuration of the different systems are varied in order to find a global minimum. As in Step 1, this involves the simulation of $r_{f0}(t)$, the calculation of the sum and difference curves $\{s(t), d(t)\}$, the convolution with an experimental response function, and the statistical analyses (χ^2, etc.). As a result of convergence one obtains the geometry configuration of the system under investigation.

were taken from ongoing experimental studies on protein structure. The application of the DDEM algorithm for analysing synthetic and real data (cf. Fig. 5.) is currently being tested.

ACKNOWLEDGMENTS

This work was financially supported by the Swedish Research Council. We are grateful to Profs. Oleg Seleznjev and Peter Olsson for advices concerning the Monte Carlo algorithm, as well as to Drs Stanislav Kalinin and Pär Håkansson for advices concerning the program used for Brownian dynamics simulations. Thanks are also extended to Mr. Erik Rosenbaum for linguistic advice.

REFERENCES

1. J.-C. Rochet and P. T. Lansbury, Jr. (2000). *Curr. Opin. Struct. Biol.* **10**, 60–68.
2. C. C. Dobson (2003). *Nature* **426**, 884–890.
3. C. L. Masters, G. Simms, N. N. Weinman, G. Multhaup, B. McDonald, and K. Beyreuther (1985). *Proc. Natl. Acad. Sci. U.S.A.* **82**, 4245–4249.
4. E. E. Egelman (1985). *J. Muscle Res. Cell Motil.* **6**, 129–151.
5. P. P. J. Moens and C. C. dos Remedios (1997). *Biochemistry* **36**, 7353–7360.
6. P. P. Stanley, V. V. Koronakis, and C. C. Hughes (1998). *Microbiol. Mol. Biol. Rev.* **62**, 309–333.
7. L. L. Abrami, M. M. Fivaz, and F. F. van der Goot (2000). *Trends Microbiol.* **8**, 168–172.
8. S. S. Wai, M. M. Westermark, J. J. Oscarsson, J. J. Jass, E. E. Maier, R. R. Benz, and B. B. Uhlin (2003). *J. Bacteriol.* **185**, 5491–5499.
9. J. J. Howard and A. A. Hyman (2003). *Nature* **422**, 753–758.
10. J. J. Lakowicz (1999). *Principles of Fluorescence Spectroscopy*, Kluwer Academic, New York.
11. B. B. Valeur (2002). *Molecular Fluorescence: Plenum Plublishers*, Wiley-VCH, New York.
12. M. M. Isaksson, S. S. Kalinin, S. S. Lobov, S. S. Wang, T. T. Ny, and L. L.-Å. Johansson (2004). *Phys. Chem. Chem. Phys.* **6**, 3001–3008.
13. L. L. -Å. Johansson, P. P. Edman, and P.-O. Westlund (1996). *J. Chem. Phys.* **105**, 10896–10904.
14. P. P. Håkansson, M. M. Isaksson, P.-O. Westlund, and L. L. -Å. Johansson (2004). *J. Phys. Chem. B* **108**, 17243–17250.
15. S. S. Scarlata, L. L. Ehrlich, and C. C. Carter (1998). *J. Mol. Biol.* **277**, 161–169.
16. J. J. Rocheleau, M. M. Edidin, and D. D. Piston (2003). *Biophys. J.* **84**, 4078–4086.
17. L. L. Erijman and G. G. Weber (1991). *Biochemistry* **30**, 1595–1599.
18. L. L. Erijman and G. G. Weber (1993). *Photochem. Photobiol.* **57**, 411–415.
19. R. R. Varma and S. S. Mayor (1998). *Nature* **394**, 798–801.
20. C. C. MacPhee, G. G. Howlett, W. W. Sawyer, and A. A. A. Clayton (1999). *Biochemistry* **38**, 10878–10884.
21. S.-T. Bogen, de Korte-Kool, G., G. G. Lindblom, and L. L. -Å. Johansson (1999). *J. Phys. Chem. B* **103**, 8344–8352.
22. R. R. Dale, J. J. Eisinger, and W. W. Blumberg (1979). *Biophys. J.* **26**, 161–194.
23. B. B. Van der Meer, G. Coker III, and S.-Y. S. Chen (1994). *Resonance Energy Transfer: Theory Data*, VCH Publishers, Germany.
24. W. W. Press, S. S. Teukolsky, and B. B. Flannery (1992). *Numerical Recipes in C*, Cambridge University Press, England.
25. D. D. Lomas, D. D. Evans, S. S. Stone, W. W. Chang, and R. R. Carell (1993). *Biochemistry* **32**, 605–607.
26. P. P. Elliot, J. J. Abrahams, and D. D. Lomas (1998). *J. Mol. Biol.* **275**, 419–425.
27. F. F. Tanaka and N. N. Mataga (1979). *Photochem. Photobiol.* **29**, 1091–1097.
28. L. L.-Å. Johansson, S. S. Engström, and M. M. Lindberg (1992). *J. Chem. Phys.* **96**, 3844–3856.